

A Two Year Time Delay for SDSS J1029+2623

Janine Fohlmeister¹

*Astronomisches Rechen-Institut, Zentrum für Astronomie der Universität Heidelberg, Mönchhofstr. 12-14,
D- 69120 Heidelberg, Germany*

Christopher S. Kochanek²

*Department of Astronomy, The Ohio State University, Columbus, OH 43210, USA
Center for Cosmology and Astroparticle Physics, The Ohio State University, 191 West Woodruff Avenue,
Columbus, OH 43210, USA*

Emilio E. Falco³

Harvard-Smithsonian Center for Astrophysics, Cambridge, MA02138, USA

Joachim Wambsganss¹

Masamune Oguri⁴

*Kavli Institute for the Physics and Mathematics of the Universe, Todai Institutes for Advanced Study,
University of Tokyo, Kashiwa, Chiba 277-8583, Japan*

Xinyu Dai⁵

Department of Physics and Astronomy, University of Oklahoma, 440 W. Brooks Street, Norman, OK 73019

ABSTRACT

We present 279 epochs of optical monitoring data spanning 5.4 years from January 2007 to June 2012 for the largest image separation ($22''.6$) gravitationally lensed quasar, SDSS J1029+2623. We find that image A leads the images B and C by $\Delta t_{AB} = (744 \pm 10)$ days, the uncertainty includes both statistical uncertainties and systematic differences due to the choice of models. With only a $\sim 1\%$ fractional error, this is in the regime where uncertainties are dominated by fluctuations in the mean line-of-sight density compared to a smooth universe rather than the measurement. We cannot separate the fainter image C from image B, but since image C trails image B by only 2–3 days in all models, the estimate of the time delay between image A and B is little affected by combining the fluxes of images B and C. There is evidence for a low level of microlensing, perhaps created by whatever satellite is responsible for the flux ratio anomaly in this system. Interpreting the delay depends on better constraining the shape of the gravitational potential using the lensed host galaxy, other lensed arcs and the structure of the X-ray emission.

Subject headings: galaxies: clusters: general — gravitational lensing: strong — quasars: individual (SDSS J102913.94+262317.9)

1. Introduction

SDSS J1029+2623 (Inada et al. 2006) is the largest image separation lensed quasar, with a maximum separation of $22''.6$ that significantly exceeds that of the next largest system ($14''.6$ for SDSS J1004+4112; Inada et al. 2003). Although it was first identified with only two images A and B, it actually consists of three images of a $z_s = 2.197$ quasar produced by a $z_l = 0.58$ galaxy cluster in a rare “naked cusp” configuration (Oguri et al. 2008). The fainter image C lies close to image B ($1''.8$), which would usually mean that B and C should be significantly brighter than A. Instead, the optical flux ratios of the images, A:B:C=0.95:1.00:0.24, show a large anomaly that cannot be reproduced by ellipsoidal models centered near the bright cluster galaxies (Oguri et al. 2008). The quasar is radio loud, and the flux ratio anomaly persists in the radio, albeit with different flux ratios than in the optical (Kratzer et al. 2011). Recent Chandra X-ray observations (Ota et al. 2012) find a cluster mass consistent with lens models and that there is soft X-ray absorption in the spectrum of image C consistent with explaining the optical color differences between the images A, B and C as extinction. After correction for this absorption/extinction, the X-ray, optical and radio flux ratios are broadly consistent with a flux ratio anomaly best explained as being due to a perturbation from an unobserved satellite (“substructure”, e.g., Kochanek & Dalal 2004) near the images B and C rather than by any additional contribution from microlensing (Kratzer et al. 2011, Ota et al. 2012).

As part of a program to better understand this system, including deep HST (Oguri et al. 2012b), X-ray (Ota et al. 2012), radio (Kratzer et al. 2011) and weak-lensing (Oguri et al. 2012a) observations, we have been monitoring the lens in the optical since 2007 to measure the time delay. Time delays generally measure a combination of cosmological distances (the Hubble constant to lowest order) and the surface density of the lens at the radius of the images (Kochanek 2002). Since the mass distribution of the lens can be independently constrained by the X-ray emission profile (Ota et al. 2012) and additional multiply imaged background galaxies of differing redshifts

from the quasar (Oguri et al. 2008), cluster lenses have the potential of being excellent cosmological probes if it can be demonstrated that the effects of substructure are controllable. Here we present a light curve for the brighter A and B images of SDSS J1029+2623 spanning six 8-month observing seasons and measure their time delay. Because image C is faint and very close to B, we cannot independently determine its delay given the quality of our images. Section §2 summarizes the available data, §3 derives the time delay, and §4 discusses the results.

2. Observations

We have monitored SDSS J1029+2623 using Keplercam at the Fred Lawrence Whipple Observatory (FLWO) 1.2m telescope over a period of 1960 days from January 2007 to June 2012 with an average sampling rate of three times a week when the source was visible. Keplercam has $0''.672$ pixels, and the 1.2m telescope presently delivers very poor quality images due to problems with its primary mirror. While the data are adequate for monitoring the widely separated A and B images, our light curve of image B is that of B and C combined. Since image C is relatively faint ($R \sim 20.3$) and expected to have a very short delay relative to image B (2–3 days, see §4), merging its flux with that of image B will have no significant consequences for our present results. Each epoch consisted of three 5 minute exposures in the r filter. The data were reduced using standard methods.

Although we analyzed the data following the methods used previously for the quintuple quasar SDSS J1004+4112 (Fohlmeister et al. 2007, Fohlmeister et al. 2008) and found consistent results, here we use the ISIS difference imaging package (Alard & Lupton 1998). The reference image shown in Figure 1 was constructed from 26 of the best quality sub-images, corresponding to a total integration time of 130 minutes. The quasar images are labeled A and B following the notation of Inada et al. (2006). The third quasar image C lies roughly $1''.8$ South of B (Oguri et al. 2008). While it is marginally resolved in the reference image, we cannot obtain a reliable, independent light curve for it. The differential light curves of A and B+C were extracted following the standard procedures for ISIS.

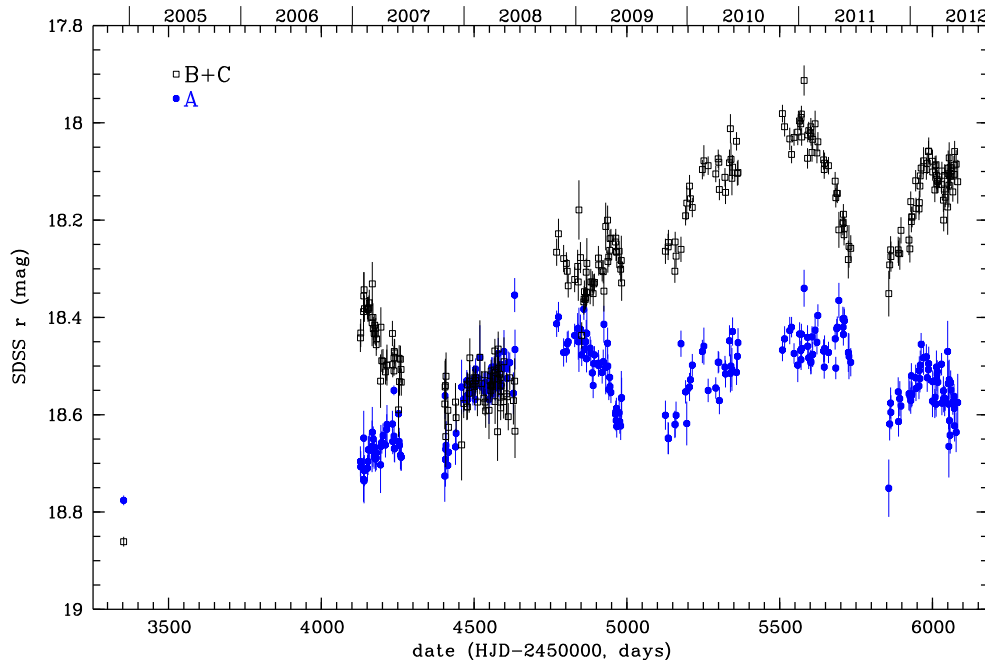


Fig. 2.— Optical r-band light curves for image A (filled blue circles) and images B+C (black squares). The first data point for both light curves is from the original SDSS observations.

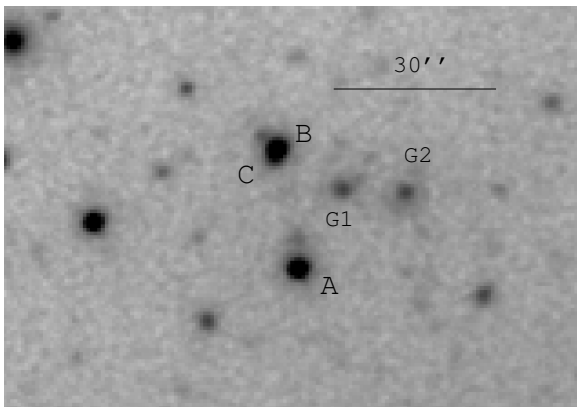


Fig. 1.— SDSS r-band Keplercam reference image of SDSS J1029+2623. This image combines 26 of the highest resolution epochs, for a total exposure time of 130 minutes. One can see that the shape of the merged images B and C is different from A.

To calibrate the reference image, we matched 39 sources in the field to stars with $15 < r < 21$ in the SDSS DR8 (Aihara et al. 2011) catalogs. We defined the zero points using the SDSS magnitudes and SExtractor (Bertin & Arnouts 1996) $5''.4$ (8 pixel) diameter aperture magnitudes for sources on the reference image. After dropping objects more than 0.1 mag from the median of the initial individual zero point estimates, the nominal uncertainties in the calibration are negligible (2 millimag). ISIS tends to modestly underestimate photometric errors. Using a combination of the light curves of stars of magnitudes comparable to those of the quasars and the statistics of points in the quasar light curves with small temporal separations,¹ we estimate that we must rescale the ISIS errors by a factor of 1.24. Combining the reference image photometry with the difference imaging light curves, we obtain the calibrated light curves presented in Table 1, where we report

¹We take three points separated by less than 7 days, predict the value of the middle points by linearly interpolating the outer points and compare the difference between the observed and predicted values of the middle point to the estimated photometric errors.

and use the rescaled error bars. Figure 2 shows the light curves. Here we have added as a first epoch the original SDSS observations of the system (Inada et al. 2006).

3. Time Delay

The challenge in measuring time delays is that the final uncertainties in essence depend on the nature of the interpolation of the light curves used for the comparison (Kundic et al. 1997). Experience demonstrates that it is worth considering multiple methods and that the formal uncertainties are typically smaller than the actual uncertainties (when tested by improved light curves, e.g., Kochanek et al. (2006) and Courbin et al. (2011) in the case of HE 0435–1223). These issues will be most problematic for short delays of the order of a few days both because the delay is not that different from the sampling cadence and because quasars show less and less variability power on shorter time scales (e.g. MacLeod et al. 2010). There is also a cosmic variance of several percent in time delays produced by fluctuations in the mean density along the line of sight (e.g. Bar-Kana 1996, Wambsganss et al. 2005), although one can attempt to use the visible galaxies in the field to estimate its amplitude (e.g. Suyu et al. 2010). Delay ratios do benefit from higher accuracy measurements because they are little affected by this cosmic variance. Because cluster lenses like SDSS J1029+2623 have relatively long delays (\sim years), it is easier to measure cosmic variance-limited delays than for single galaxy lenses.

Here we determine the time delays between images A and the combined B+C image pair, where we know from simply shifting the light curves by hand that the delay is on the order of two years. We first consider two methods that do not directly test for microlensing or model its effects. If we first consider the cross-correlation method described in Fohlmeister et al. (2007), we measure a delay of $\Delta t_{AB} = (746 \pm 6)$ days (all delays are in the sense of A leading B). The dispersion method of Pelt et al. (1994) and Pelt et al. (1996) gives a delay of $\Delta t_{AB} = (745 \pm 10)$ days. The Kochanek et al. (2006) polynomial method, where the source light curve and microlensing magnifications are described by polynomials, lets

us examine the effects of microlensing. We modeled each season with polynomials of all orders from $N_s = 3$ to 25 and with constant, linear or quadratic ($N_\mu = 1$ to 3) polynomials for the microlensing variability in each season.

Models allowing for no microlensing were strongly ruled out by the data. We evaluate the models using Bayesian information criteria to weight the changes in the numbers of parameters between models, where the probability of a delay with a goodness of fit χ^2 is $\exp(-\chi^2/2 - kN_p)$ where $N_p = 4(N_s + N_\mu)$ is the number of parameters in the model.² We consider both the more liberal Akaike information criterion (AIC) with $k = 1$, and the more conservative Bayesian information criterion (BIC) with $k = \ln N_{data}$ (see Poindexter et al. 2007), where $N_{data} = 355$ is the number of data points in the seasons that overlap. The AIC favors $N_s \sim 7$ and $N_\mu = 2$ (formally, the relative probabilities for $N_\mu = 1, 2$ and 3 are 0.19 : 1.00 : 0.11), while the BIC favors $N_s \simeq 5$ and $N_\mu = 1$ (1.0 : 0.0 : 0.0). The combined result for the AIC is a median time delay of $\Delta t_{AB} = 740.0$ with a 90% confidence range of $739.0 < \Delta t_{AB} < 744.9$, while that for the BIC is a median of $\Delta t_{AB} = 748.6$ with a 90% confidence range of $742.6 < \Delta t_{AB} < 753.8$. As Figure 3 shows, it is difficult to evaluate the relative merits of these solutions by eye, although the low order polynomials favored by the BIC seem to overly smooth the light curves independent of their statistical merits. If we apply no information criterion at all, the median is $t_{AB} = 739.3$ with a 90% confidence range of $730.8 < t_{AB} < 744.5$.

If we consider the two most probable models, $N_s = 7$ and $N_\mu = 2$ for the AIC and $N_s = 5$ and $N_\mu = 1$ for the BIC, we find that the effects of microlensing are small but statistically significant. In the best BIC model, the flux ratios in the four seasons are $\Delta m_{AB} = -0.373 \pm 0.006$, -0.413 ± 0.006 , -0.424 ± 0.005 and -0.384 ± 0.006 mag for the four overlapping seasons. The small fluctuations suggest the presence of microlensing, with the middle two seasons showing a significant shift of about 0.05 mag relative to the first and last seasons. AIC model shifts are very similar but have marginally

²Each of the four “seasons” is described by a source polynomial of order N_s and a microlensing polynomial of order N_μ .

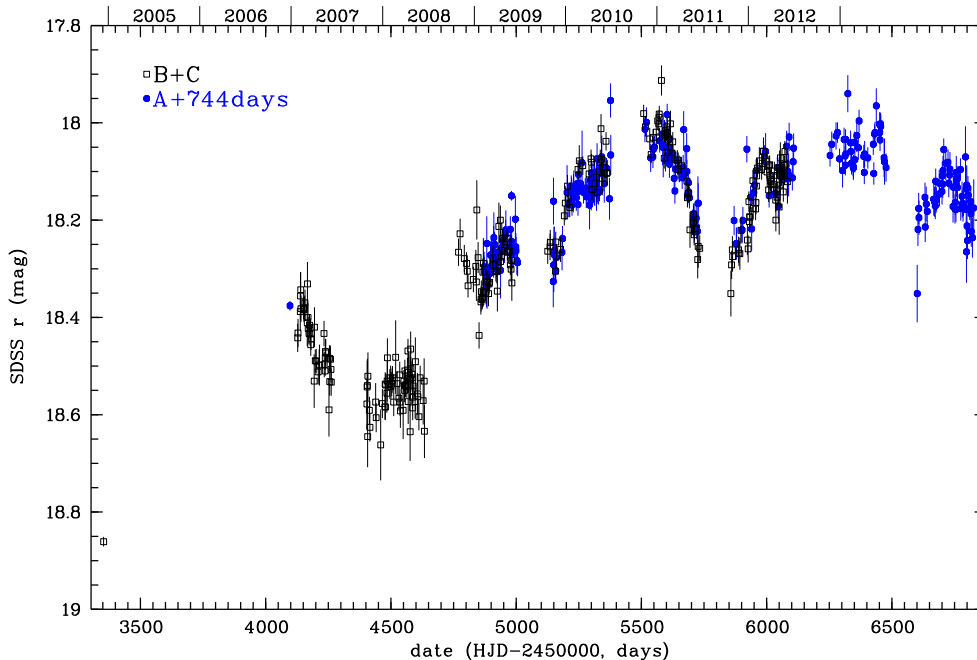


Fig. 3.— Light curves for image A (filled blue circles) and images B+C (black squares) after shifting image A by the estimated time delay of $\Delta t_{AB} = (744 \pm 10)$ days and -0.40 mag. While not included in the models, note that the data point for A from the original SDSS observations, shown by the blue circle at the start of the light curves, matches well the start of our light curve for image B+C.

detected gradients of -0.04 ± 0.06 , -0.03 ± 0.03 , 0.08 ± 0.03 and -0.07 ± 0.04 mag/year. Given the quality of the data, these effects are not obvious, and it is not inconceivable that they are partly due to systematics from matching data taken at very different epochs even though ISIS excels at properly cross calibrating data and correcting for PSF differences. In fact, when we fit the light curves of stars with similar magnitudes, there were also shifts of this amplitude, so the detection of microlensing is marginal.

Figure 4 shows the lightcurves of the A and B+C images shifted by the determined time delay of $\Delta t_{AB} = (744 \pm 10)$ days and -0.40 mag. The shifted photometry for image A from the original SDSS observations in 2004 closely matches the start of our light curves although it is not quite overlapping. The later R-band observations by Oguri et al. (2008) are contemporaneous with the start of our observations, so we lack any additional data in the gap between 2004 and 2007.

4. Summary and Discussion

We presented 5.4 years of optical monitoring for the two bright lensed quasar images of the largest image separation gravitationally lensed quasar SDSS J1029+2623. We find that image A leads the images B and C by $\Delta t_{AB} = (744 \pm 10)$ days. The formal error bar on the time delay which includes statistical uncertainties and systematic differences, is $\sim 1.3\%$ and is in the regime where uncertainties are dominated by fluctuations in the mean line-of-sight density. We find that the effect of microlensing in this system is small but statistically significant. This is the second longest measured time delay after the 822 day delay between images C and A in SDSS J1004+4112 (Fohlmeister et al. 2008).

A detailed interpretation of the measured delay is deferred pending the completion of our analysis of the HST images (Oguri et al. 2012b) and additional spectroscopy of the lensed arcs in this system. However, as an experiment, we fit the lens using an NFW model centered on galaxy G2 with

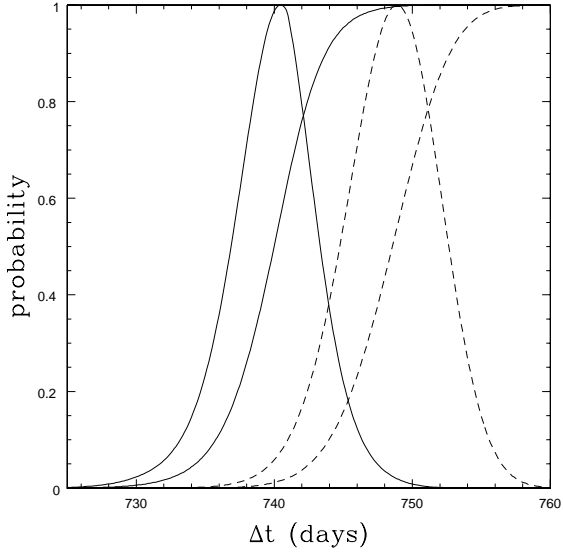


Fig. 4.— Polynomial method probability distributions for the time delay based on either the AIC (solid) or BIC (dashed) information criteria for combining the models. Both the differential and integral probability distributions are shown, with the differential probability normalized to its maximum.

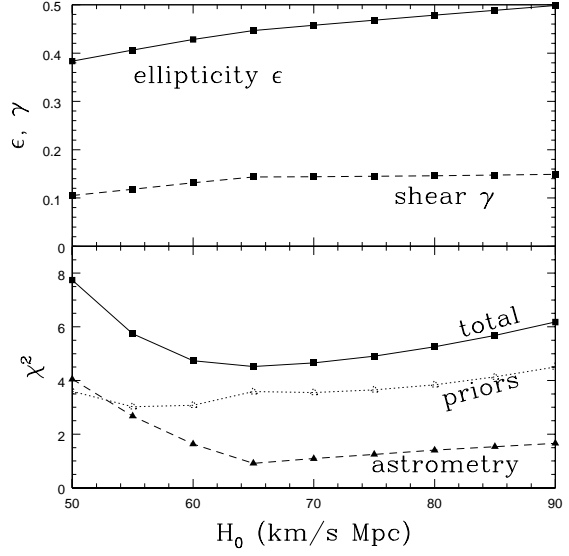


Fig. 5.— Goodness of fit as a function of the Hubble constant H_0 for simple models consisting of an ellipsoidal NFW model in an external shear. The solid line (black squares) show the total χ^2 statistic for the goodness of fit, which is dominated by contributions from the image positions (astrometry, filled triangles, dashed curve) and the ellipticity and lens position priors (priors, open triangles, dotted curves) with negligible contributions from matching the time delays. The upper panels show the trend of the models towards flatter density distributions, where the axis ratio of the model is $1 - \epsilon$, and higher external shear γ for increasing H_0 .

a break radius of $78''$ based on the X-ray data (Ota et al. 2012). We adopt the component positions ($\pm 0''.05$) from (Oguri et al. 2008) and a time delay of $\Delta t_{AB} = (744 \pm 10)$ days that tries to conservatively combine the AIC and BIC results. We used priors of $\pm 1''$ on the position of the model relative to galaxy G2, $\epsilon = 0.46 \pm 0.05$ for the ellipticity of the cluster density, and $\gamma = 0.05 \pm 0.05$ for any additional external shear. The value of ϵ was determined by the best fit model with $H_0 = 70 \text{ km s}^{-1} \text{ Mpc}^{-1}$. We then fit models as a function of the Hubble constant H_0 assuming a flat, $\Omega_0 = 0.3$, and $\Lambda_0 = 0.7$ cosmological model. We did not include the flux ratios in the fits because of the known flux ratio anomaly. The anomaly appears to be due to a small galaxy near image C (Oguri et al. 2012b) which should have little effect on the overall geometry and the AB time delay. In a normal four-image lens, the constraint on the radial mass profile from the X-ray data would largely eliminate any degeneracies because they are created by uncertainties in the surface mass density at the radius of the images (Kochanek 2002).

Fig. 5 shows the resulting goodness of fit as a function of H_0 for these simple models. Low values of H_0 are disfavored by the astrometry, while high values are weakly disfavored by the priors on the shape of the potential. There is clearly a strong need for additional constraints in order to use this delay for the full characterization of the lens system. There is certainly no difficulty improving the astrometric constraints, since with HST it will be trivial to increase the astrometric precision from the $0''.05$ used here to $0''.01$ or smaller, although the concern here will be whether noise from unmodeled sub-structures in the cluster dominate over the measurement precision. More important, however, is the addition of strong constraints on the shape of the potential, since there is a strong trend requiring flatter density distributions and higher external shears for larger values of H_0 . We already know from Oguri et al. (2008) that there is a lensed image of the quasar host galaxy as well as several additional arc systems, and this is confirmed by the new HST observations (Oguri et al. 2012b). Particularly if combined with additional arc redshifts and direct mass models of the X-ray emission, there are no obvious barriers to greatly improving on Fig. 5. Where Suyu et al. (2010) use dynamical measurements of the central lens

galaxy to break the Kochanek (2002) or other degeneracies, here we should be able to do so using a combination of the X-ray and arc data. There is, however, significant evidence that the cluster is undergoing a merger, which means that the additional lensing constraints will be more reliable constraints on the mass distribution than further X-ray observations. On the other hand, the ability to combine deeper X-ray observations with the lensing constraints makes this system an excellent laboratory for studying the effects of mergers on the X-ray properties of clusters.

In our present data, measuring the B-C time delay is impossible given the data quality. It does shift steadily over the model sequence, decreasing with increasing H_0 from 3.4 to 2.1 days. This fully justifies our making the measurements using the combined B/C light curve. It is well worth measuring the BC delay because it is very sensitive to the perturbing galaxy that causes the flux ratio anomaly (see Oguri 2007, Keeton & Moustakas 2009) and hence probes the structure of galaxy halos in cluster environments. Such short delays are extremely difficult to measure accurately in ground based observations because quasars have so little variability power on such short time scales (see Mushotzky et al. 2011) and might require a space-based lens monitoring satellite like the proposed OMEGA (Moustakas et al. 2008).

We thank all the participating observers at the Harvard-Smithsonian Center for Astrophysics for their support of these observations. Our observations were obtained with the F. L. Whipple 1.2m telescope, with support from the Smithsonian Astrophysical Observatory. CSK is supported by NSF grant AST-1009756. This work was supported in part by the FIRST program “Subaru Measurements of Images and Redshifts (SuMIRe)”, World Premier International Research Center Initiative (WPI Initiative), MEXT, Japan, and Grant-in-Aid for Scientific Research from the JSPS (23740161). Funding for SDSS-III has been provided by the Alfred P. Sloan Foundation, the Participating Institutions, the National Science Foundation, and the U.S. Department of Energy Office of Science. The SDSS-III web site is <http://www.sdss3.org/>. SDSS-III is managed by the Astrophysical Research Consortium for the Participating Institutions of the

SDSS-III Collaboration including the University of Arizona, the Brazilian Participation Group, Brookhaven National Laboratory, University of Cambridge, Carnegie Mellon University, University of Florida, the French Participation Group, the German Participation Group, Harvard University, the Instituto de Astrofísica de Canarias, the Michigan State/Notre Dame/JINA Participation Group, Johns Hopkins University, Lawrence Berkeley National Laboratory, Max Planck Institute for Astrophysics, New Mexico State University, New York University, Ohio State University, Pennsylvania State University, University of Portsmouth, Princeton University, the Spanish Participation Group, University of Tokyo, University of Utah, Vanderbilt University, University of Virginia, University of Washington, and Yale University.

REFERENCES

- Aihara, H., Allende Prieto, C., An, D., et al. 2011, *ApJS*, 193, 29
- Alard, C., & Lupton, R. H. 1998, *ApJ*, 503, 325
- Bar-Kana, R. 1996, *ApJ*, 468, 17
- Bertin, E., & Arnouts, S. 1996, *A&AS*, 117, 393
- Courbin, F., Chantry, V., Revaz, Y., et al. 2011, *A&A*, 536, A53
- Fohlmeister, J., Kochanek, C. S., Falco, E. E., et al. 2007, *ApJ*, 662, 62
- Fohlmeister, J., Kochanek, C. S., Falco, E. E., Morgan, C. W., & Wambsganss, J. 2008, *ApJ*, 676, 761
- Inada, N., Oguri, M., Pindor, B., et al. 2003, *Nature*, 426, 810
- Inada, N., et al. 2006, *ApJ*, 653, L97
- Keeton, C. R., & Moustakas, L. A. 2009, *ApJ*, 699, 1720
- Kochanek, C. S. 2002, *ApJ*, 578, 25
- Kochanek, C. S., & Dalal, N. 2004, *ApJ*, 610, 69
- Kochanek, C. S., Morgan, N. D., Falco, E. E., McLeod, B. A., Winn, J. N., Dembicky, J., & Ketzeback, B. 2006, *ApJ*, 640, 47
- Kratzer, R. M., et al. 2011, *ApJ*, 728, L18
- Kundic, T., Turner, E. L., Colley, W. N., et al. 1997, *ApJ*, 482, 75
- MacLeod, C. L., Ivezić, Ž., Kochanek, C. S., et al. 2010, *ApJ*, 721, 1014
- Moustakas, L. A., Bolton, A. J., Booth, J. T., et al. 2008, *Proc. SPIE*, 7010
- Mushotzky, R. F., Edelson, R., Baumgartner, W., & Gandhi, P. 2011, *ApJ*, 743, L12
- Oguri, M. 2007, *ApJ*, 660, 1
- Oguri, M., et al. 2008, *ApJ*, 676, L1
- Oguri, M., Bayliss, M. B., Dahle, H., et al. 2012, *MNRAS*, 420, 3213
- Oguri, M., et al. 2012, in preparation
- Ota, N., Oguri, M., Dai, X., et al. 2012, *arXiv:1202.1645*
- Pelt, J., Hoff, W., Kayser, R., Refsdal, S., & Schramm, T. 1994, *A&A*, 286, 775
- Pelt, J., Kayser, R., Refsdal, S., & Schramm, T. 1996, *A&A*, 305, 97
- Poindexter, S., Morgan, N., Kochanek, C. S., & Falco, E. E. 2007, *ApJ*, 660, 146
- Suyu, S. H., Marshall, P. J., Auger, M. W., et al. 2010, *ApJ*, 711, 201
- Wambsganss, J., Bode, P., Ostriker, J. P., 2005, *ApJ*, 635, 1

TABLE 1
LIGHT CURVES

HJD-2450000	A (mag)	B(+C) (mag)
3352.900	18.776 \pm 0.010	18.861 \pm 0.010
4127.878	18.696 \pm 0.031	18.442 \pm 0.029
4128.910	18.707 \pm 0.032	18.432 \pm 0.029
4137.945	18.733 \pm 0.046	18.388 \pm 0.038
4138.794	18.648 \pm 0.056	18.356 \pm 0.049
4139.819	18.736 \pm 0.046	18.343 \pm 0.036
4140.835	18.715 \pm 0.032	18.382 \pm 0.027
4150.891	18.710 \pm 0.027	18.381 \pm 0.023
4152.773	18.696 \pm 0.028	18.384 \pm 0.025
4153.772	18.672 \pm 0.028	18.383 \pm 0.025
4155.860	18.672 \pm 0.028	18.380 \pm 0.025
4156.841	18.671 \pm 0.032	18.370 \pm 0.027
4165.937	18.665 \pm 0.053	18.411 \pm 0.048
4166.780	18.636 \pm 0.052	18.331 \pm 0.045
4168.873	18.675 \pm 0.032	18.400 \pm 0.029
4169.826	18.650 \pm 0.026	18.423 \pm 0.024
4172.730	18.687 \pm 0.024	18.433 \pm 0.022
4174.794	18.667 \pm 0.025	18.416 \pm 0.023
4176.867	18.691 \pm 0.026	18.434 \pm 0.024
4177.805	18.685 \pm 0.023	18.422 \pm 0.021
4179.682	18.689 \pm 0.025	18.456 \pm 0.023
4180.702	18.678 \pm 0.025	18.444 \pm 0.023
4193.775	18.703 \pm 0.058	18.531 \pm 0.055
4194.814	18.665 \pm 0.044	18.420 \pm 0.041
4197.741	18.657 \pm 0.023	18.489 \pm 0.023
4201.799	18.643 \pm 0.025	18.490 \pm 0.025
4209.686	18.662 \pm 0.026	18.512 \pm 0.026
4213.818	18.630 \pm 0.031	18.498 \pm 0.032
4214.667	18.620 \pm 0.040	18.498 \pm 0.042
4232.721	18.619 \pm 0.027	18.433 \pm 0.026
4233.753	18.655 \pm 0.026	18.497 \pm 0.026
4237.500	18.550 \pm 0.010	18.510 \pm 0.010
4237.688	18.644 \pm 0.025	18.483 \pm 0.025
4238.703	18.670 \pm 0.027	18.470 \pm 0.026
4239.760	18.669 \pm 0.029	18.473 \pm 0.028
4252.658	18.598 \pm 0.048	18.590 \pm 0.055
4254.675	18.655 \pm 0.028	18.484 \pm 0.027
4255.683	18.663 \pm 0.028	18.532 \pm 0.029
4258.690	18.683 \pm 0.029	18.486 \pm 0.028
4260.712	18.687 \pm 0.028	18.507 \pm 0.027
4261.698	18.687 \pm 0.028	18.533 \pm 0.028
4404.003	18.726 \pm 0.053	18.578 \pm 0.052
4405.003	18.561 \pm 0.048	18.543 \pm 0.054
4405.981	18.692 \pm 0.056	18.540 \pm 0.055
4407.006	18.671 \pm 0.057	18.645 \pm 0.063
4407.993	18.663 \pm 0.050	18.521 \pm 0.049
4414.021	18.704 \pm 0.027	18.591 \pm 0.028
4416.001	18.677 \pm 0.027	18.626 \pm 0.029
4439.043	18.666 \pm 0.037	18.574 \pm 0.039
4440.999	18.638 \pm 0.026	18.606 \pm 0.030
4459.013	18.543 \pm 0.056	18.662 \pm 0.073
4466.002	18.568 \pm 0.026	18.577 \pm 0.030
4475.979	18.530 \pm 0.022	18.584 \pm 0.027
4477.013	18.534 \pm 0.021	18.537 \pm 0.024
4477.955	18.560 \pm 0.022	18.584 \pm 0.026
4478.977	18.569 \pm 0.022	18.539 \pm 0.024
4483.849	18.550 \pm 0.034	18.556 \pm 0.040
4484.941	18.542 \pm 0.037	18.531 \pm 0.042
4485.951	18.535 \pm 0.037	18.483 \pm 0.040

TABLE 1—*Continued*

HJD-2450000	A (mag)	B(+C) (mag)
4495.906	18.554 \pm 0.027	18.537 \pm 0.031
4498.900	18.542 \pm 0.022	18.524 \pm 0.025
4499.883	18.525 \pm 0.022	18.542 \pm 0.025
4502.989	18.568 \pm 0.023	18.537 \pm 0.025
4504.919	18.506 \pm 0.022	18.530 \pm 0.025
4505.958	18.532 \pm 0.021	18.524 \pm 0.024
4510.952	18.524 \pm 0.024	18.574 \pm 0.029
4518.867	18.482 \pm 0.066	18.482 \pm 0.076
4524.882	18.543 \pm 0.023	18.536 \pm 0.026
4531.700	18.536 \pm 0.022	18.566 \pm 0.026
4534.946	18.534 \pm 0.023	18.518 \pm 0.027
4535.786	18.552 \pm 0.023	18.574 \pm 0.028
4537.630	18.539 \pm 0.028	18.592 \pm 0.035
4548.789	18.569 \pm 0.050	18.591 \pm 0.059
4551.717	18.518 \pm 0.020	18.531 \pm 0.023
4553.846	18.544 \pm 0.023	18.540 \pm 0.027
4554.645	18.526 \pm 0.020	18.550 \pm 0.024
4555.642	18.559 \pm 0.021	18.510 \pm 0.023
4557.804	18.503 \pm 0.021	18.539 \pm 0.024
4558.726	18.502 \pm 0.020	18.539 \pm 0.023
4560.751	18.532 \pm 0.020	18.542 \pm 0.023
4565.831	18.502 \pm 0.022	18.508 \pm 0.025
4567.789	18.545 \pm 0.024	18.469 \pm 0.025
4568.779	18.523 \pm 0.037	18.573 \pm 0.046
4569.707	18.535 \pm 0.036	18.513 \pm 0.042
4575.724	18.519 \pm 0.044	18.527 \pm 0.050
4576.730	18.534 \pm 0.047	18.635 \pm 0.060
4577.771	18.511 \pm 0.040	18.526 \pm 0.045
4578.768	18.474 \pm 0.032	18.465 \pm 0.036
4579.698	18.541 \pm 0.022	18.505 \pm 0.024
4583.680	18.499 \pm 0.023	18.517 \pm 0.027
4584.703	18.543 \pm 0.025	18.524 \pm 0.029
4585.747	18.537 \pm 0.021	18.564 \pm 0.024
4586.699	18.539 \pm 0.021	18.586 \pm 0.025
4587.683	18.497 \pm 0.021	18.551 \pm 0.025
4588.648	18.540 \pm 0.021	18.541 \pm 0.024
4596.739	18.504 \pm 0.029	18.573 \pm 0.035
4597.703	18.470 \pm 0.044	18.491 \pm 0.050
4605.654	18.505 \pm 0.036	18.557 \pm 0.043
4607.679	18.525 \pm 0.039	18.563 \pm 0.046
4611.712	18.492 \pm 0.022	18.604 \pm 0.028
4616.671	18.493 \pm 0.021	18.524 \pm 0.025
4628.648	18.556 \pm 0.043	18.571 \pm 0.049
4632.651	18.354 \pm 0.035	18.531 \pm 0.047
4633.655	18.466 \pm 0.041	18.634 \pm 0.055
4769.958	18.413 \pm 0.027	18.266 \pm 0.028
4776.021	18.399 \pm 0.031	18.228 \pm 0.031
4793.023	18.472 \pm 0.029	18.279 \pm 0.028
4801.948	18.470 \pm 0.023	18.289 \pm 0.023
4804.847	18.454 \pm 0.025	18.305 \pm 0.025
4807.942	18.450 \pm 0.023	18.335 \pm 0.024
4829.042	18.437 \pm 0.024	18.322 \pm 0.026
4838.864	18.423 \pm 0.032	18.295 \pm 0.034
4840.957	18.450 \pm 0.037	18.327 \pm 0.039
4842.930	18.446 \pm 0.066	18.179 \pm 0.061
4847.995	18.424 \pm 0.030	18.277 \pm 0.032
4851.991	18.477 \pm 0.023	18.437 \pm 0.027
4859.020	18.383 \pm 0.022	18.368 \pm 0.026
4859.999	18.466 \pm 0.024	18.362 \pm 0.026

TABLE 1—*Continued*

HJD-2450000	A (mag)	B(+C) (mag)
4861.001	18.450 \pm 0.022	18.347 \pm 0.023
4863.932	18.450 \pm 0.019	18.363 \pm 0.021
4864.895	18.450 \pm 0.021	18.359 \pm 0.022
4866.841	18.432 \pm 0.027	18.307 \pm 0.028
4867.868	18.485 \pm 0.028	18.349 \pm 0.029
4868.854	18.433 \pm 0.051	18.289 \pm 0.052
4879.646	18.463 \pm 0.024	18.348 \pm 0.025
4882.028	18.473 \pm 0.027	18.327 \pm 0.027
4886.686	18.514 \pm 0.023	18.327 \pm 0.022
4889.620	18.540 \pm 0.026	18.351 \pm 0.026
4891.858	18.495 \pm 0.020	18.331 \pm 0.020
4893.874	18.477 \pm 0.018	18.328 \pm 0.018
4906.858	18.494 \pm 0.027	18.278 \pm 0.025
4907.657	18.499 \pm 0.023	18.292 \pm 0.022
4918.854	18.513 \pm 0.023	18.304 \pm 0.022
4922.675	18.491 \pm 0.025	18.306 \pm 0.024
4924.785	18.414 \pm 0.038	18.346 \pm 0.042
4930.757	18.503 \pm 0.055	18.213 \pm 0.049
4936.810	18.453 \pm 0.032	18.200 \pm 0.030
4937.655	18.500 \pm 0.024	18.285 \pm 0.023
4940.663	18.548 \pm 0.022	18.276 \pm 0.020
4943.649	18.523 \pm 0.021	18.262 \pm 0.020
4944.683	18.542 \pm 0.021	18.238 \pm 0.018
4947.703	18.554 \pm 0.022	18.237 \pm 0.019
4962.657	18.599 \pm 0.022	18.245 \pm 0.019
4963.658	18.594 \pm 0.023	18.237 \pm 0.019
4964.670	18.612 \pm 0.022	18.265 \pm 0.019
4965.672	18.587 \pm 0.022	18.264 \pm 0.019
4966.675	18.624 \pm 0.023	18.266 \pm 0.019
4974.679	18.596 \pm 0.025	18.264 \pm 0.021
4976.685	18.614 \pm 0.025	18.292 \pm 0.021
4979.673	18.623 \pm 0.029	18.301 \pm 0.026
4981.679	18.566 \pm 0.056	18.283 \pm 0.051
4982.720	18.565 \pm 0.041	18.329 \pm 0.037
5125.985	18.601 \pm 0.030	18.264 \pm 0.026
5135.020	18.648 \pm 0.033	18.255 \pm 0.027
5136.013	18.649 \pm 0.032	18.246 \pm 0.026
5157.029	18.620 \pm 0.028	18.305 \pm 0.024
5157.997	18.620 \pm 0.026	18.245 \pm 0.021
5160.956	18.601 \pm 0.028	18.274 \pm 0.024
5177.026	18.454 \pm 0.027	18.260 \pm 0.026
5192.028	18.553 \pm 0.024	18.191 \pm 0.020
5195.977	18.618 \pm 0.045	18.165 \pm 0.035
5204.997	18.543 \pm 0.029	18.130 \pm 0.023
5208.020	18.528 \pm 0.024	18.156 \pm 0.020
5214.035	18.498 \pm 0.023	18.174 \pm 0.020
5246.959	18.470 \pm 0.024	18.096 \pm 0.020
5251.857	18.459 \pm 0.038	18.078 \pm 0.032
5265.907	18.550 \pm 0.024	18.088 \pm 0.019
5290.785	18.545 \pm 0.022	18.105 \pm 0.017
5298.764	18.492 \pm 0.023	18.074 \pm 0.019
5300.794	18.492 \pm 0.021	18.081 \pm 0.017
5302.645	18.571 \pm 0.028	18.137 \pm 0.022
5320.794	18.502 \pm 0.023	18.112 \pm 0.019
5322.797	18.516 \pm 0.028	18.143 \pm 0.024
5335.696	18.448 \pm 0.032	18.082 \pm 0.027
5338.680	18.515 \pm 0.039	18.012 \pm 0.030
5340.669	18.500 \pm 0.043	18.075 \pm 0.034
5343.675	18.507 \pm 0.044	18.114 \pm 0.035

TABLE 1—*Continued*

HJD-2450000	A (mag)	B(+C) (mag)
5345.657	18.429 \pm 0.029	18.091 \pm 0.025
5358.654	18.513 \pm 0.026	18.038 \pm 0.019
5361.665	18.480 \pm 0.030	18.104 \pm 0.025
5363.681	18.452 \pm 0.030	18.102 \pm 0.026
5509.008	18.467 \pm 0.023	17.981 \pm 0.018
5516.029	18.444 \pm 0.026	18.008 \pm 0.020
5533.044	18.427 \pm 0.028	18.033 \pm 0.023
5538.857	18.420 \pm 0.021	18.065 \pm 0.018
5547.002	18.474 \pm 0.021	18.030 \pm 0.017
5559.060	18.498 \pm 0.035	18.019 \pm 0.027
5565.041	18.434 \pm 0.024	17.996 \pm 0.019
5569.048	18.468 \pm 0.020	18.002 \pm 0.015
5570.034	18.487 \pm 0.021	17.989 \pm 0.015
5571.054	18.434 \pm 0.021	17.982 \pm 0.017
5572.017	18.464 \pm 0.022	18.029 \pm 0.018
5580.062	18.340 \pm 0.038	17.913 \pm 0.031
5591.053	18.441 \pm 0.025	18.073 \pm 0.021
5591.810	18.459 \pm 0.019	18.025 \pm 0.015
5594.990	18.483 \pm 0.023	18.016 \pm 0.018
5600.907	18.489 \pm 0.021	18.021 \pm 0.016
5602.016	18.493 \pm 0.024	18.008 \pm 0.018
5602.742	18.491 \pm 0.025	18.028 \pm 0.019
5605.987	18.440 \pm 0.022	18.061 \pm 0.019
5608.030	18.476 \pm 0.026	18.034 \pm 0.020
5616.008	18.426 \pm 0.034	18.002 \pm 0.027
5621.979	18.451 \pm 0.025	18.062 \pm 0.021
5624.972	18.396 \pm 0.023	18.039 \pm 0.020
5643.645	18.469 \pm 0.024	18.076 \pm 0.020
5645.839	18.502 \pm 0.024	18.096 \pm 0.019
5646.917	18.464 \pm 0.027	18.083 \pm 0.022
5659.832	18.472 \pm 0.022	18.088 \pm 0.018
5681.640	18.444 \pm 0.022	18.120 \pm 0.019
5683.704	18.504 \pm 0.023	18.154 \pm 0.020
5686.721	18.423 \pm 0.020	18.145 \pm 0.018
5688.639	18.420 \pm 0.022	18.145 \pm 0.020
5693.706	18.365 \pm 0.036	18.220 \pm 0.037
5706.738	18.403 \pm 0.025	18.207 \pm 0.024
5707.682	18.420 \pm 0.024	18.204 \pm 0.022
5708.680	18.435 \pm 0.023	18.188 \pm 0.021
5710.662	18.402 \pm 0.023	18.230 \pm 0.022
5711.660	18.407 \pm 0.024	18.217 \pm 0.024
5724.679	18.472 \pm 0.040	18.281 \pm 0.039
5726.666	18.480 \pm 0.047	18.254 \pm 0.044
5732.664	18.492 \pm 0.029	18.258 \pm 0.027
5857.014	18.751 \pm 0.059	18.351 \pm 0.047
5860.003	18.619 \pm 0.034	18.292 \pm 0.029
5863.007	18.576 \pm 0.032	18.261 \pm 0.028
5863.982	18.595 \pm 0.035	18.275 \pm 0.031
5887.995	18.553 \pm 0.030	18.261 \pm 0.027
5889.027	18.614 \pm 0.031	18.268 \pm 0.026
5893.027	18.567 \pm 0.036	18.269 \pm 0.033
5897.037	18.582 \pm 0.031	18.221 \pm 0.027
5923.052	18.557 \pm 0.034	18.241 \pm 0.031
5926.044	18.562 \pm 0.031	18.259 \pm 0.028
5929.049	18.571 \pm 0.027	18.162 \pm 0.021
5931.046	18.520 \pm 0.026	18.203 \pm 0.022
5932.046	18.560 \pm 0.025	18.193 \pm 0.021
5933.046	18.557 \pm 0.025	18.194 \pm 0.021
5945.038	18.524 \pm 0.027	18.119 \pm 0.022

TABLE 1—*Continued*

HJD-2450000	A (mag)	B(+C) (mag)
5946.030	18.546 \pm 0.026	18.176 \pm 0.022
5955.988	18.541 \pm 0.027	18.177 \pm 0.023
5957.052	18.509 \pm 0.029	18.164 \pm 0.024
5959.050	18.526 \pm 0.028	18.130 \pm 0.023
5960.050	18.498 \pm 0.030	18.109 \pm 0.025
5963.050	18.455 \pm 0.023	18.093 \pm 0.020
5971.008	18.483 \pm 0.035	18.078 \pm 0.028
5979.929	18.481 \pm 0.026	18.096 \pm 0.021
5983.010	18.524 \pm 0.029	18.083 \pm 0.022
5986.995	18.507 \pm 0.028	18.059 \pm 0.022
5987.671	18.495 \pm 0.035	18.058 \pm 0.028
5999.900	18.572 \pm 0.033	18.079 \pm 0.024
6000.801	18.532 \pm 0.023	18.101 \pm 0.018
6007.905	18.577 \pm 0.030	18.138 \pm 0.025
6008.890	18.564 \pm 0.026	18.088 \pm 0.020
6011.836	18.578 \pm 0.026	18.086 \pm 0.019
6012.958	18.502 \pm 0.034	18.108 \pm 0.028
6013.904	18.527 \pm 0.025	18.125 \pm 0.020
6014.855	18.517 \pm 0.023	18.116 \pm 0.019
6015.829	18.511 \pm 0.023	18.120 \pm 0.019
6017.719	18.533 \pm 0.031	18.120 \pm 0.024
6029.686	18.496 \pm 0.023	18.127 \pm 0.019
6030.756	18.576 \pm 0.025	18.099 \pm 0.019
6035.876	18.551 \pm 0.030	18.159 \pm 0.024
6036.763	18.567 \pm 0.028	18.200 \pm 0.023
6038.694	18.566 \pm 0.025	18.136 \pm 0.019
6039.849	18.573 \pm 0.030	18.108 \pm 0.023
6041.695	18.567 \pm 0.025	18.153 \pm 0.020
6049.845	18.470 \pm 0.063	18.173 \pm 0.057
6051.684	18.536 \pm 0.047	18.093 \pm 0.036
6052.683	18.578 \pm 0.052	18.105 \pm 0.039
6053.684	18.665 \pm 0.064	18.128 \pm 0.046
6054.688	18.528 \pm 0.041	18.072 \pm 0.032
6055.717	18.612 \pm 0.039	18.109 \pm 0.029
6057.760	18.642 \pm 0.038	18.092 \pm 0.028
6059.686	18.534 \pm 0.025	18.110 \pm 0.020
6060.668	18.549 \pm 0.024	18.099 \pm 0.018
6066.656	18.574 \pm 0.026	18.142 \pm 0.020
6070.655	18.562 \pm 0.025	18.087 \pm 0.019
6071.655	18.587 \pm 0.028	18.106 \pm 0.021
6072.655	18.623 \pm 0.032	18.059 \pm 0.022
6077.661	18.636 \pm 0.041	18.085 \pm 0.029
6082.659	18.575 \pm 0.059	18.121 \pm 0.045

NOTE.—The first point is the original SDSS observation from December 2004 (Inada et al. 2006). The Keplercam observations started in January 2007. The uncertainties are dominated by the noise in the individual epochs rather than the photometric calibration.